PCCP

COMMUNICATION

View Article Online
View Journal

Cite this: DOI: 10.1039/d5cp04903b

Received 17th December 2025,
Accepted 23rd April 2026

DOI: 10.1039/d5cp04903b

rsc.li/pccp

Quasi-solid electrolytes using a single-cation ionic liquid

Yuta Ito,* Keigo Kubota, Yuta Maeyoshi, Toyoki Okumura and Kazuki Yoshii*

Proof-of-concept quasi-solid electrolytes (QSEs) combining $Li_{1+x+y}Al_xTi_{2-x}Si_yP_{3-y}O_{12}$ and a single-cation ionic liquid (SCIL) composed of lithium bis(fluorosulfonyl)amide and lithium (fluorosulfonyl)(trifluoromethanesulfonyl)amide are demonstrated without inducing concentration gradients. The QSEs exhibited ionic conductivities comparable to the SCIL without high-temperature sintering. These results demonstrate the potential of SCIL-based QSEs as model systems for investigating Li^+ transport under concentration-gradient-free conditions in solid-state battery systems.

Rechargeable batteries are essential for a decarbonized society. However, conventional lithium-ion batteries use flammable organic electrolytes, raising safety, cost, and recycling concerns.[1–4] Solid electrolytes (SEs), which eliminate ignition risks,[5] are typically composed of sulfides,[6] oxides,[7] halides,[8] and polymers.[9] Oxide SEs such as garnet-type $Li_7La_3Zr_2O_{12}$ (LLZO),[10] LISICON-type $Li_{4-2x}Zn_xGeO_4$,[11] and NASICON-type $Li_{1+x}Al_xTi_{2-x}(PO_4)_3$ (LATP)[12,13] offer high ionic conductivity (10^{-4}–10^{-3} S cm^{-1} at room temperature) with good electrochemical stability. Yet, their poor interfacial contact requires high-temperature processing.[14,15]

Quasi-solid electrolytes (QSEs) have been widely investigated as an effective strategy to improve interfacial contact between SEs as well as between SEs and active materials by incorporating soft materials such as ionic liquids (ILs) or polymers, thereby enhancing processability.[14–17] However, despite these advantages, the ionic conductivities of many IL- or polymer-based QSEs remain lower than those of sintered SE pellets.[14–17] Moreover, under electrochemical polarization, ion transport in such soft-material-containing QSEs is often accompanied by concentration polarization originating from the mobile ionic species in the soft phase, including not only anions but also organic cations present in room-temperature ILs. This concentration polarization can obscure intrinsic ion-transport behavior in composite electrolytes and hinders reliable evaluation of Li^+ transport, particularly across solid–soft material interfaces. From this perspective, the development of QSEs based on soft materials that do not induce concentration polarization is highly desirable, as it would provide a well-defined model system for examining ion-transport behavior in composite electrolytes without complications arising from concentration gradients.

Single cation ionic liquids (SCILs),[18–20] which contain only one type of alkali cation such as Li^+ (though analogous systems exist for Na^+ and K^+), represent a class of soft materials in which Li^+ is the sole mobile cation. Because they do not induce concentration polarization under anion-blocking conditions, SCILs provide a suitable model soft material for QSE systems in which ion-transport behavior can be evaluated without complications arising from concentration gradients. We have previously reported a Li-based SCIL composed of lithium bis(fluorosulfonyl)amide (LiFSA) and lithium (fluorosulfonyl)-(trifluoromethanesulfonyl)amide (LiFTA), with a chemical composition of $Li[FSA]_{0.35}[FTA]_{0.65}$, which exhibits a reduced melting point (76 °C) and high electrochemical stability.[21]

In this study, we designed a model QSE system by combining LATP with the SCIL described above, thereby providing Li^+-dominant transport in both phases. This material design minimizes concentration polarization and allows ion-transport properties of the composite electrolyte to be evaluated under well-defined conditions. Furthermore, by comparing this system with a composite incorporating a non-Li^+-conductive oxide and the same SCIL, we examined how the presence of a Li^+-conductive solid phase affects ion-transport behavior in QSEs, beyond simple percolation of the ionic liquid. This work provides a proof-of-concept for QSE systems in which ion transport can be investigated under concentration-gradient-free conditions, highlighting the utility of SCIL-based electrolytes as model platforms for fundamental studies of ion transport in composite electrolytes.

In this study, the QSEs were prepared by mixing LATP with x wt% SCIL (x = 0, 1, 5, 10, 17, 25, 33, and 50) followed by hot pressing at 90 °C (Fig. 1a). However, the sample containing

Research Institute of Electrochemical Energy, Department of Energy and Environment, National Institute of Advanced Industrial Science and Technology (AIST), 1-8-31 Midorigaoka, Ikeda, Osaka 563-8577, Japan.
E-mail: ito.yuta@aist.go.jp, k.yoshii@aist.go.jp

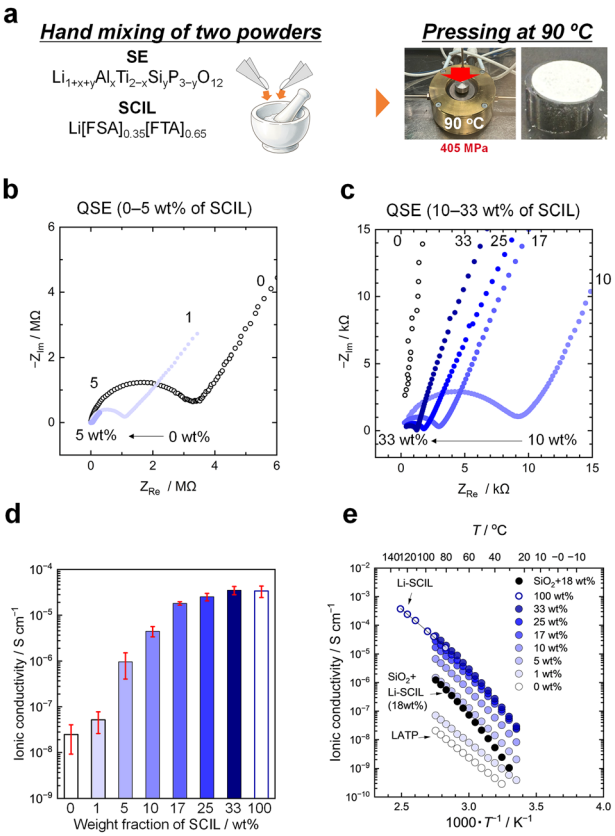

Fig. 1 (a) Schematic illustration of the preparation of QSEs by mixing and pressing LATP and SCIL ($Li[FSA]_{0.35}[FTA]_{0.65}$). (b) and (c) Nyquist plots of QSEs composed of LATP and x wt% SCIL measured at 90 °C: (b) x = 0, 1, and 5; (c) x = 10, 17, 25, and 33. (d) Ionic conductivity of QSEs and SCIL at 90 °C. Error bars represent standard deviations of three independent measurements (N = 3). (e) Arrhenius plots of QSEs prepared by mixing LATP with x wt% SCIL (x = 0–33). The data were collected during cooling from 90 °C to 25 °C.

50 wt% SCIL failed to form a self-standing QSE and was therefore excluded from subsequent electrochemical measurements.

The thickness, volume, and porosity of the QSEs are summarized in Table S1. Electrochemical impedance spectroscopy (EIS) was performed at selected temperature steps. Specifically, the sample was heated from 25 °C to 90 °C, cooled to −10 °C, and finally returned to 25 °C, with 2 h equilibration at each temperature (Fig. S1).

Fig. 1b and c show the Nyquist plots of the QSEs measured at 90 °C. The LATP sample without SCIL exhibits low ionic conductivity, which is attributed to the characteristics of unsintered LATP systems, where inter-particle resistance dominates ion transport.[22] In the present system, the impedance response is governed by inter-particle and grain boundary resistance, and the bulk resistance could not be reliably separated due to the absence of a clearly resolved high-frequency intercept. Therefore, only the total resistance was used for conductivity evaluation.

The ionic conductivity at 90 °C is summarized in Fig. 1d, where error bars represent the standard deviation of three independent measurements (N = 3). The ionic conductivity of the QSE with 33 wt% SCIL is $3.5 \times 10^{-5} \pm 7.2 \times 10^{-6}$ S cm^{-1}, which is comparable to that of SCIL alone ($3.4 \times 10^{-5} \pm 9.5 \times 10^{-6}$ S cm^{-1}) within experimental uncertainty. These results indicate that the incorporation of LATP does not degrade the intrinsic ionic conductivity of the SCIL. The ionic conductivity values as a function of temperature are summarized in Table S2.

A slight increase in conductivity at higher SCIL contents cannot be excluded. However, the observed difference falls within the experimental uncertainty and does not provide conclusive evidence for a strong synergistic effect between the SE and the SCIL. Instead, the conductivity enhancement relative to pristine LATP is primarily attributed to the formation of continuous ion-conduction pathways mediated by the SCIL phase.

Nevertheless, the ionic conductivity of the present QSE remains lower than that of sintered LATP. This can be attributed to incomplete densification due to the absence of high-temperature sintering and the lack of continuous, fast Li^+ conduction pathways within the LATP phase. Instead, ion transport is governed by non-ideal percolation through the composite structure. The formation of a highly conductive interfacial layer at the SE/IL interface may also be limited. In contrast to sintered ceramics, the present system is designed to enable mechanical formability without high-temperature processing and improving ionic conductivity while maintaining this advantage remains an important challenge for future work.

Fig. 1e presents the Arrhenius plots of ionic conductivity for the LATP–SCIL QSEs together with that of a SiO_2–SCIL composite. A noticeable change in the apparent activation energy is observed with increasing SCIL content in LATP–SCIL QSEs. At low SCIL contents, ion transport is dominated by the inter-particle resistance of LATP, resulting in lower activation energy. With increasing SCIL content, the contribution of the SCIL phase becomes more significant, resulting in higher activation energy. This trend suggests a gradual transition in the dominant ion transport pathways as the composition changes, although the exact contributions of each pathway cannot be quantitatively determined from the present data.

The Arrhenius plots of SiO_2-based system exhibit pronounced curvature, characteristic of Vogel–Tammann–Fulcher-type behavior. Since SiO_2 is not a Li^+ conductor, ion transport in this system is expected to occur mainly through the SCIL phase and interfacial regions. In this system, the SCIL content is 18 wt%, corresponding to a volume fraction of 20 vol%. This volume fraction is identical to that of the LATP-based QSE with 17 wt% SCIL. In contrast, the LATP–SCIL QSEs exhibit higher ionic conductivity under comparable conditions. This difference suggests that ion transport in the LATP-based QSEs cannot be fully explained by SCIL percolation alone, and that the presence of a Li^+-conductive solid phase influences the overall transport behavior.

Although Li^+ transport in QSEs can proceed through multiple pathways, including transport through the SCIL phase, along solid–liquid interfaces, and potentially through the SE

bulk, the present results do not allow a definitive identification of the dominant pathway. However, the comparison with the SiO_2-based system indicates that contributions beyond simple SCIL percolation are likely involved. Notably, the QSEs exhibit enhanced ionic conductivity even below the melting point of SCIL (76 °C), which may be associated with a supercooled state of the SCIL phase.[23]

The ionic conductivity increased with increasing SCIL content and reached the highest value at 33 wt%. A marked increase was observed at SCIL contents of 17 wt% and above compared to lower concentrations (0–10 wt%). Considering both electrochemical performance and mechanical properties, the QSE with 17 wt% SCIL exhibited improved conductivity while maintaining good machinability and structural integrity. Therefore, 17 wt% was selected as the representative composition for further characterization.

Fig. 2a shows changes in the thickness of the QSEs. Both samples containing 0 and 17 wt% SCIL became thinner after pressing at 90 °C, with a more pronounced reduction observed for the 17 wt% sample. This behavior is attributed to SCIL melting during hot pressing, leading to redistribution of SCIL within the composite. The pellet thickness remained nearly unchanged after EIS measurements, indicating that the use of the pre-measured thickness introduces negligible error in conductivity calculations.

X-ray diffraction patterns (Fig. 2b) confirm that the crystal structure of LATP remains unchanged after hot pressing, indicating chemical stability. Peaks corresponding to solid-state SCIL decreased after hot pressing, consistent with its melting behavior. Differential scanning calorimetry (Fig. S3) shows an endothermic peak corresponding to SCIL melting[21] without additional thermal events.

Scanning electron microscopy combined with energy-dispersive X-ray analysis (Fig. 2c–e and Fig. S4–S6) reveals that large Li-salt particles (>20 μm) observed at 25 °C disappear after hot pressing. In addition, F and S elements become uniformly distributed. These results indicate that molten SCIL spreads within the QSEs, fills voids, and contributes to densification.

Fig. 3a shows the chronoamperogram of a Li/separator/QSE (17 wt% SCIL)/separator/Li cell under 10 mV polarization at 90 °C. The corresponding Nyquist plots before and after polarization are shown in Fig. 3b. Separators impregnated with SCIL were used to isolate ion transport within the QSE from interfacial reactions with Li metal. The polarization current shows minimal decay, indicating that the current is predominantly sustained by Li^+ transport with negligible contribution from concentration polarization. No significant increase in resistance is observed after polarization, suggesting stable interfacial behavior under the present conditions.

Related approaches using single-ion conducting polymers combined with inorganic SEs have also been explored to mitigate concentration gradients.[24,25] However, these systems typically involve more complex ion transport environments and may not fully suppress concentration gradients. In contrast, the present SCIL-based system enables investigation of ion transport behavior under conditions where concentration polarization is effectively suppressed.

This study demonstrates a proof-of-concept QSE of an oxide SE (LATP) and a Li-based SCIL, fabricated without

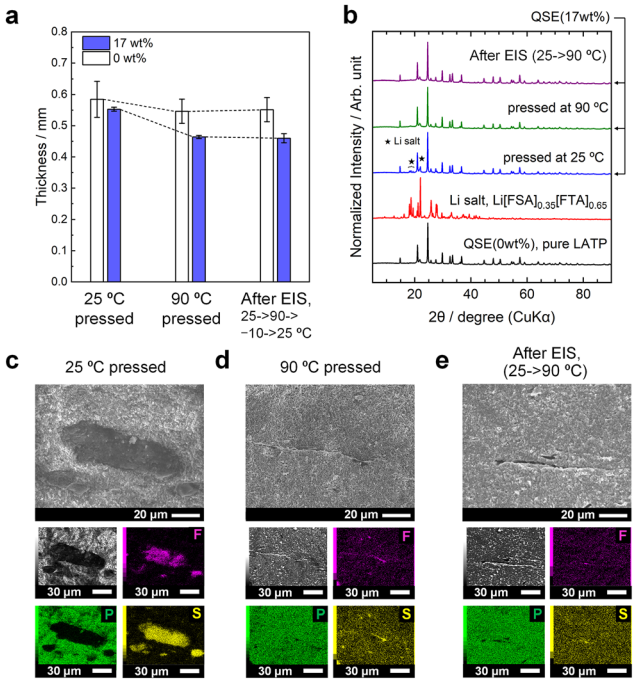

Fig. 2 (a) Thicknesses of QSEs containing 0 and 17 wt% SCIL, prepared by pressing at 25 °C, pressing at 90 °C, and pressing at 90 °C followed by temperature-dependent EIS measurements at 25 °C → 90 °C → −10 °C → 25 °C. (b) XRD patterns of (i) QSE (0 wt%, namely pure LATP), (ii) SCIL ($Li[FSA]_{0.35}[FTA]_{0.65}$) and QSE (17 wt%) pressed under three conditions: (1) at 25 °C with SCIL in the solid state, (2) at 90 °C, and (3) at 90 °C after temperature-dependent EIS measurements at 25 °C → 90 °C. The results confirm the absence of structural changes of LATP in the QSE after hot pressing and subsequent EIS measurement. (c)–(e) Cross-sectional SEM images and corresponding EDX mappings of the pellets in states (1)–(3), respectively.

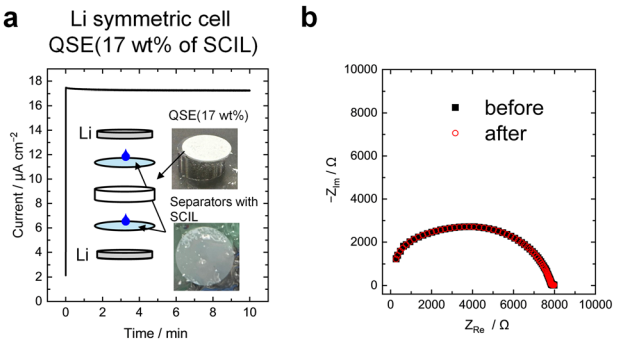

Fig. 3 (a) Chronoamperogram of a Li/separator/QSE (17 wt% SCIL)/separator/Li cell obtained under 10 mV polarization measured at 90 °C. (b) The Nyquist plots acquired before and after polarization. The separators were impregnated with SCIL.

high-temperature sintering. The resulting QSEs exhibit ionic conductivity comparable to that of SCIL and improving the processability and mechanical integrity.

Comparison with a SiO_2–SCIL system indicates that ion transport in the LATP-based QSE cannot be fully explained solely by simple SCIL percolation, suggesting a contribution from the Li^+-conductive solid phase. DC polarization measurements further suggest that concentration polarization is suppressed under the present measurement conditions.

Although the ionic conductivity remains lower than that of sintered LATP,[26–28] this approach provides a model platform for fundamental studies of ion transport in composite electrolytes. Future work should focus on improving SCIL conductivity, optimizing SE materials, and reducing interfacial resistance. Moreover, a detailed understanding of ion transport phenomena at the SCIL/SE interfaces is essential for rationally designing high-performance QSEs.

Author contributions

Y. I.: methodology, validation, formal analysis, investigation (fabrication of QSE, electrochemical measurements, XRD, SEM observation and EDX analysis), data curation (SI), writing – original draft, visualization (Fig. 1–3). K. K.: Investigation (DSC and density measurement), writing – review & editing. Y. M.: resources (electrochemical measurement device), writing – review & editing. T. O.: writing – review & editing, project administration, funding acquisition. K. Y.: conceptualization, methodology, writing – review & editing, visualization (Fig. 1), supervision, project administration, funding acquisition.

Conflicts of interest

There are no conflicts to declare.

Data availability

Supplementary information (SI): structural information of QSEs, photographs of QSEs, Arrhenius plots, detailed results of SEM observation and EDX analysis. See DOI: https://doi.org/10.1039/d5cp04903b.

Acknowledgements

We thank Yoshiko Yamazaki for her technical assistance in the preparation of QSEs, including measurements of ionic conductivity, SEM observations, EDX analysis, photographic documentation of QSEs, and partial analysis of EIS data. This work was supported by the JST GteX Program (Grant Number JPMJGX23S2).

References

1 D. H. Doughty, E. P. Roth, C. C. Crafts, G. Nagasubramanian, G. Henriksen and K. Amine, *J. Power Sources*, 2005, **146**, 116–120.
2 W. Li, H. Wang, Y. Zhang and M. Ouyang, *J. Energy Storage*, 2019, **24**, 100775.
3 A. Sevarin, M. Fasching, M. Raffler and C. Ellersdorfer, *Batteries*, 2023, **9**, 195.
4 S. Wu, N. Kaden and K. Dröder, *Batteries*, 2023, **9**, 297.
5 Z. Chen, K. Wang, P. Pei, Y. Zuo, M. Wei, H. Wang, P. Zhang and N. Shang, *Nano Res.*, 2022, **16**, 2311–2324.
6 G. Kumar Mishra, M. Gautam, K. Bhawana, C. Sah Kalwar, M. Patro, A. Yadav and S. Mitra, *Chemistry*, 2024, **30**, e202402510.
7 M. Umair, S. Zhou, W. Li, H. T. H. Rana, J. Yang, L. Cheng, M. Li, S. Yu and J. Wei, *Batteries Supercaps*, 2024, **8**, e202400667.
8 R. Xu, Y. Wu, Z. Dong, R. Zheng, Z. Song, Z. Wang, H. Sun, Y. Liu and L. Zhang, *Nano Energy*, 2024, **132**, 110435.
9 N. G. Ningappa, A. K. Madikere Raghunatha Reddy and K. Zaghib, *Batteries*, 2024, **10**, 454.
10 Y. Zhang, F. Chen, R. Tu, Q. Shen and L. Zhang, *J. Power Sources*, 2014, **268**, 960–964.
11 P. G. Bruce and A. R. West, *Mater. Res. Bull.*, 1980, **15**, 379–385.
12 H. Aono, E. Sugimoto, Y. Sadaoka, N. Imanaka and G. Y. Adachi, *J. Electrochem. Soc.*, 1989, **136**, 590–591.
13 S. Duluard, A. Paillassa, L. Puech, P. Vinatier, V. Turq, P. Rozier, P. Lenormand, P.-L. Taberna, P. Simon and F. Ansart, *J. Eur. Ceram. Soc.*, 2013, **33**, 1145–1153.
14 H. W. Kim, P. Manikandan, Y. J. Lim, J. H. Kim, S.-C. Nam and Y. Kim, *J. Mater. Chem. A*, 2016, **4**, 17025–17032.
15 H. Junoh, N. Awang, H. S. Zakria, N. A. S. Zainuddin, N. Nordin, N. S. Suhaimin, T. Enoki, T. Uno and M. Kubo, *Materials*, 2024, **17**, 4344.
16 L. Xu, J. Li, H. Shuai, Z. Luo, B. Wang, S. Fang, G. Zou, H. Hou, H. Peng and X. Ji, *J. Energy Chem.*, 2022, **67**, 524–548.
17 D. M. Reinoso, C. de la Torre-Gamarra, A. J. Fernandez-Ropero, B. Levenfeld and A. Varez, *ACS Appl. Energy Mater.*, 2024, **7**, 1527–1538.
18 H. Yamamoto, C. Y. Chen, K. Kubota, K. Matsumoto and R. Hagiwara, *J. Phys. Chem. B*, 2020, **124**, 6341–6347.
19 H. Yamamoto, K. Kubota, J. Hwang, K. Matsumoto and R. Hagiwara, *J. Phys. Chem. B*, 2025, **129**, 3652–3660.
20 L. Schkeryantz, P. Nguyen, W. D. McCulloch, C. E. Moore, K. C. Lau and Y. Wu, *J. Phys. Chem. C*, 2022, **126**, 11407–11413.
21 Y. Ito, K. Kubota, Y. Maeyoshi, T. Okumura and K. Yoshii, *J. Phys. Chem. C*, 2025, **129**, 9656–9661.
22 A. Méry, S. Rousselot, D. Lepage, D. Aymé-Perrot and M. Dollé, *Batteries*, 2023, **9**, 87.

23 K. Kubota and H. Matsumoto, *Chem. Lett.*, 2011, **40**, 1105–1106.
24 M. Lechartier, L. Porcarelli, H. Zhu, M. Forsyth, A. Guéguen, L. Castro and D. Mecerreyes, *Mater. Adv.*, 2022, **3**, 1139–1151.
25 L. W. Tian, J. W. Kim, D. Xie, W. Li and D.-W. Kim, *Mater. Today Energy*, 2025, **54**, 102128.
26 K. Kwatek, W. Ślubowska, C. Ruiz, I. Sobrados, J. Sanz, J. E. Garbarczyk and J. L. Nowiński, *J. Alloys Compd.*, 2020, **838**, 155623.
27 F. Öksüzoğlu, Ş. Ateş, O. M. Özkendir, G. Çelik, Y. R. Eker and H. Baveghar, *Ceram. Int.*, 2024, **50**, 31435–31441.
28 H. Aono, E. Sugimoto, Y. Sadaoka, N. Imanaka and G. Y. Adachi, *J. Electrochem. Soc.*, 1990, **137**, 1023–1027.